

Combined Spectroscopic/Computational Studies of Metal Centers in Proteins and Cofactors: Application to Coenzyme B₁₂

Thomas C. Brunold*
Werner Prize Winner 2003

Abstract: This article illustrates how the combined computational/spectroscopic methodology used in our studies of metal centers in proteins and cofactors can be applied to vitamin B₁₂ and its biologically relevant derivatives. The B₁₂ cofactors have long fascinated chemists because of their complex structures and unusual reactivities in biological systems; however, their electronic absorption (Abs) spectra have remained largely unassigned. In this study, Abs, circular dichroism (CD), magnetic CD (MCD), and resonance Raman spectroscopic techniques are used to probe the electronic excited states of various Co³⁺Cbl species that differ with respect to their upper axial ligand. Spectroscopic data for each species are analyzed within the framework of time-dependent density functional theory (TD-DFT) to assign the major spectral features and to generate experimentally validated bonding descriptions. A simple model is presented that explains why the identity of the upper axial ligand has a major effect on the Co–N_{ax} bond strength, whereas the lower axial ligand does not appreciably modulate the nature of the Co–C bond. Implications of these results with respect to enzymatic Co–C bond activation are discussed.

Keywords: Bioinorganic chemistry · Coenzyme B₁₂ · Density functional theory · Metalloenzymes · Spectroscopy



Thomas C. Brunold was born in Bern, Switzerland, in 1969. He received his PhD from the University of Bern in 1996, working with Hans U. Güdel on the design and spectroscopic characterization of new transition-metal based near-IR laser materials. From 1997 to 1999, he was a postdoctoral fellow with Edward I.

Solomon at Stanford University, studying binuclear iron and manganese centers in proteins and synthetic model complexes. He joined the faculty at the University of Wisconsin-Madison in 1999, where his research interests include spectroscopic and computational studies on superoxide dismutases and Fe-, Co-, and Ni-containing enzymes and cofactors that form organometallic reaction intermediates.

1. Introduction

The B₁₂ cofactors methylcobalamin (MeCbl) and 5'-deoxyadenosylcobalamin (AdoCbl) have long fascinated chemists with their complex structures (Fig. 1) and unusual reactivities in biological systems [2–6]. Cobalamins possess a low-spin Co³⁺ center ligated equatorially by the four nitrogens of a highly substituted macrocycle (the corrin ring) and axially coordinated by a nitrogen from the tethered base 5,6-dimethylbenzimidazole (DMB) [7]. A wide range of ligands can occupy the upper axial position, such as CN, H₂O, Me, and Ado; however, only MeCbl and AdoCbl are enzymatically competent [8][9]. The MeCbl-dependent enzymes catalyze methyl-transfer reactions through *heterolytic* cleavage of the cofactor's Co–C bond, yielding a protein-bound Co¹⁺Cbl species [10–12]. Alternatively, enzymes utilizing AdoCbl catalyze radical-induced rearrangement reactions *via homolytic* cleavage of the Co–C bond to produce Co²⁺Cbl and an organic radical centered on the 5'-carbon of the Ado moiety [9][13–17]. This Ado• radical then serves to abstract a hydrogen atom from substrate as the first step in a protein-mediated substrate rearrangement reaction. B₁₂-dependent enzymes activate the

organometallic Co–C bond to a spectacular degree; a rate enhancement for bond homolysis by as much as 12 orders of magnitude has been reported for some enzymes [18–21].

Despite extensive studies of the B₁₂ cofactors, fundamental questions regarding their electronic properties and reactivities remain largely unanswered. Electronic absorption (Abs) and circular dichroism (CD) spectroscopic techniques have been used extensively to probe changes in the geometric and electronic properties of the cofactor upon protein binding [22–24], but the lack of a suitable theoretical framework within which to interpret these changes greatly limited progress toward elucidation of enzymatic Co–C bond activation mechanisms on the basis of spectroscopic data.

A 'typical' Co³⁺Cbl Abs spectrum (Fig. 2, top) is dominated by two features, the so-called α/β bands in the visible spectral region and the γ band in the UV. Several additional, considerably weaker features termed D and E bands are sometimes observed between the α/β and γ bands, the origin of which remained controversial. Such 'typical' Abs spectra are observed for nearly all Co³⁺Cbl species, such as vitamin B₁₂ (cyanocobalamin, CNCbl) and aquacobalamin (H₂Ocbl⁺), in which the upper axial

*Correspondence: Prof. T.C. Brunold
Department of Chemistry
1101 University Avenue
University of Wisconsin
Madison, WI 53706, USA
Tel.: +1 608 265 9056
Fax: +1 608 262 6143
E-Mail: brunold@chem.wisc.edu
<http://www.chem.wisc.edu/main/people/faculty/brunold.html>

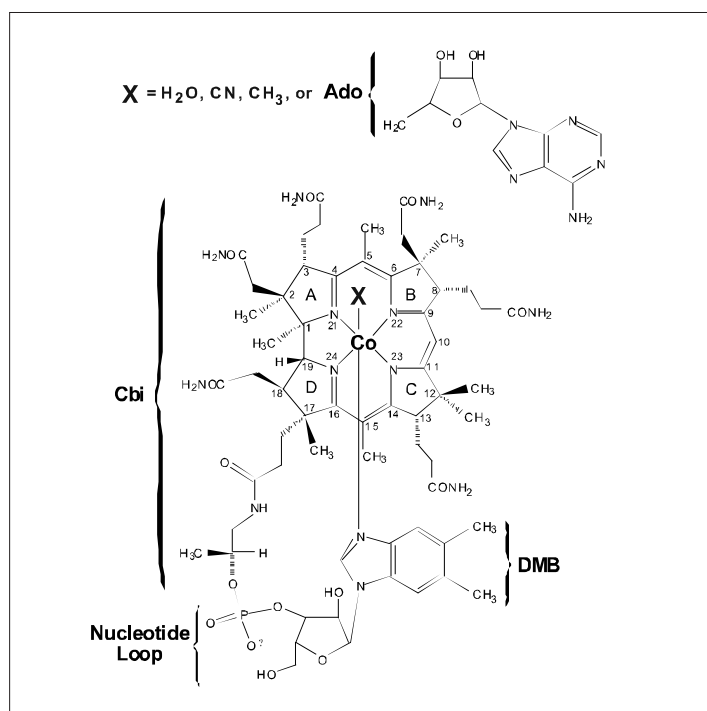


Fig. 1. Chemical structure and numbering scheme for $\text{Co}^{3+}\text{Cbls}$, where X indicates the upper axial ligand. Reprinted with permission from [1]. Copyright 2003 American Chemical Society.

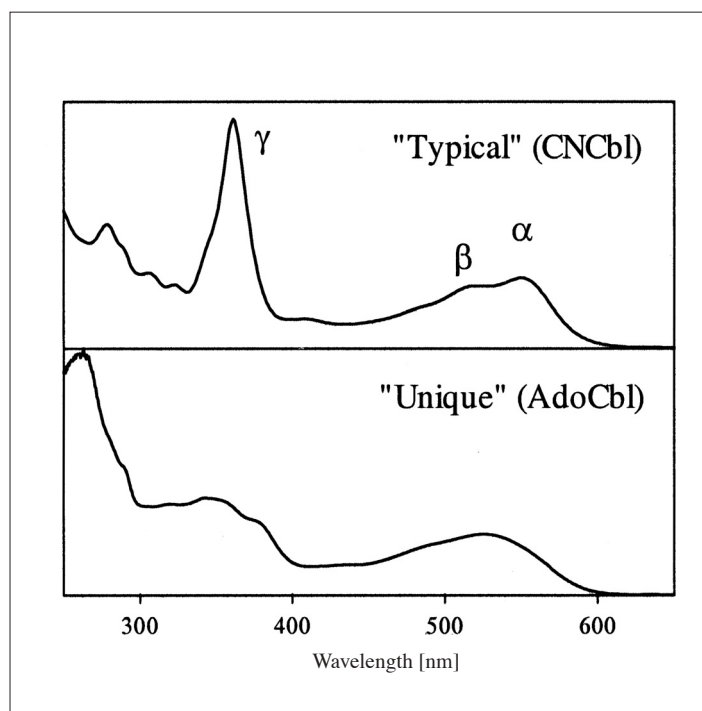


Fig. 2. Room temperature Abs spectra for aqueous solutions of CNCbl (top) and AdoCbl (bottom). Band designations are indicated in the 'typical' CNCbl Abs spectrum. Reprinted with permission from [1]. Copyright 2003 American Chemical Society.

position is occupied by cyanide and water molecules, respectively (Fig. 1) [23][25]. In contrast, alkylcobalamins, such as MeCbl and AdoCbl, exhibit 'unique' Abs spectra that differ from 'typical' spectra in several ways (Fig. 2, top and bottom). Most strikingly, the intensity of the γ band in the 'unique' spectra is redistributed over several similarly intense transitions in the UV spectral region. The fact that the Co^{3+}Cbl Abs spectrum varies as a function of the 'upper' axial ligand even though it is dominated by corrin $\pi \rightarrow \pi^*$ transitions suggests that the axial ligands and the corrin macrocycle are electronically coupled; however, the mechanism by which this coupling occurs remained largely unexplored.

This article, which is based on a recent publication from our laboratory [1], illustrates how the combined spectroscopic/computational methodology used in our research can be applied to vitamin B_{12} and its biologically relevant derivatives. Abs, CD, magnetic CD (MCD), and resonance Raman (RR) spectroscopic data are presented for a representative set of Co^{3+}Cbl species whose upper axial ligands span the spectrochemical series, including MeCbl, AdoCbl, CNCbl, and H_2OCbl^+ . Spectroscopic data are analyzed within the framework of time-dependent density functional theory (TD-DFT) to assign key electronic transitions and to generate quantitative bonding descriptions. These studies permit detailed insight into the factors that distinguish $\text{Co}^{3+}\text{Cbls}$ exhibiting a 'typical' Abs spectrum from those displaying a

'unique' spectrum and afford a simple model that explains why the identity of the upper axial ligand has a major effect on the $\text{Co}-\text{N}_{\text{ax}}$ bond strength, whereas the lower axial ligand does not appreciably modulate the nature of the $\text{Co}-\text{C}$ bond.

2. Spectroscopic/Computational Methodology

The combined spectroscopic/computational methodology employed in our research on metal centers in proteins and cofactors is based largely on the pioneering work of Solomon and coworkers [26][27]. The Table provides an overview of the methods used in our laboratory and the insights they provide into geometric and electronic structure. Several recent developments have been crucial to the success of our research; e.g. the vast improvements in computer technology that now permit DFT calculations to be performed on realistic active-site and cofactor models and the establishment of a theoretical framework by Neese and Solomon for the quantitative analysis of VTVH-MCD data for systems with spin $S \geq 1/2$ (Table) [28].

3. Results and Analysis

3.1. Spectroscopic Data

3.1.1. Abs, CD, and MCD

Fig. 3 shows Abs, CD, and MCD spectra of three different Co^{3+}Cbl species, in-

cluding MeCbl, H_2OCbl^+ , and CNCbl (vitamin B_{12}) [1]. Consistent with the diamagnetic ground state of $\text{Co}^{3+}\text{Cbls}$ (i.e. the Co^{3+} center has a low-spin $3d^6$ electron configuration), all features in the MCD spectra of Fig. 3 were found to be temperature independent.

H_2OCbl^+ : The Abs spectrum of H_2OCbl^+ (Fig. 3B, top) shows the three sets of bands that characterize a 'typical' Co^{3+}Cbl spectrum: the α/β bands previously assigned as the origin and a vibrational sideband of the corrin-based HOMO \rightarrow LUMO (i.e. $\pi \rightarrow \pi^*$) transition polarized along the long axis of the corrin macrocycle ($\text{C}^5 \cdots \text{C}^{15}$ vector, Fig. 1) [25][29]; the D/E bands that are relatively well resolved for this particular species; and the γ band attributed to a corrin $\pi \rightarrow \pi^*$ transition polarized along the short corrin axis ($\text{Co} \cdots \text{C}^{10}$ vector) [25][29]. The α/β region of the CD spectrum (Fig. 3B, center) exhibits one band of large negative intensity that coincides with the α band in the Abs spectrum and several weak features of positive intensity, one of which occurs at lower energy than the α band. In the MCD spectrum (Fig. 3B, bottom) a single weak feature is observed in this region that coincides with the α band. The D/E bands coincide with the two negative features in the corresponding region of the MCD spectrum, whereas in the CD spectrum two relatively intense features that are offset relative to the D/E bands (and, thus, must be associated with different electronic transitions) are observed in this region. Lastly, the γ region of

Table. Overview of spectroscopic and computational methods employed in our bioinorganic research^a

Method	Obtainable Parameters	Information Content
Ground State		
Electron Paramagnetic Resonance (EPR)	g values; axial (D) and rhombic (E) zero-field splittings (ZFS)	Spin of ground state; ligand field (LF) splittings of metal 3d orbitals and their relative covalencies
	Hyperfine couplings	Spin distribution within molecule
Variable-temperature/variable-field Magnetic Circular Dichroism (VTVH MCD)	g values; ZFS parameters	See EPR above
	Transition polarizations	Identification of ligand(s) involved in charge transfer (CT) transitions
Resonance Raman (RR)	Vibrational frequencies	Force constants
	Isotope shifts	Band assignments; binding mode of exogenous ligands
Excited States		
Electronic Absorption (Abs)	Transition energies and intensities (oscillator strengths)	LF splittings of metal 3d orbitals; metal–ligand bond covalencies; relative energies of metal/ligand orbitals
	Band shapes	Excited-state distortions
Circular Dichroism (CD)	Transition energies and intensities (rotational strengths)	Same as Abs; resolution of overlapping bands in Abs spectrum, magnetic-dipole character of transition
Magnetic CD (MCD)	Transition energies and intensities (A, B, and C terms)	Same as Abs; resolution of overlapping Abs bands, nature of excited states
	C/D ratio (\propto MCD/Abs intensity)	Metal character in transition
Computations		
Density Functional Theory (DFT)	Energy-minimized metric parameters	Structures and energies of hypothetical active-site models
	Molecular orbital (MO) energies and compositions	Quantitative bonding description
Time-dependent (TD) DFT	Predicted transition energies and Abs intensities	Aids in evaluating hypothetical active-site models
Semi-empirical INDO/S-CI	Predicted Spin Hamiltonian parameters (g values, D, and E) and transition energies and Abs intensities	Same as TD-DFT
^a See [26] and [27] for excellent reviews of the spectroscopic methods typically employed in bioinorganic research.		

the CD spectrum contains contributions from at least two transitions, as evidenced by the presence of two positive CD features in this region.

CNCbl: The Abs, CD, and MCD spectra of CNCbl (Fig. 3C) exhibit the same basic features as those of H₂OCbl⁺; however, with several subtle differences. The α band is red-shifted by 760 cm⁻¹ to 18080 cm⁻¹, and there is no indication for the presence of a low-energy feature similar to the one observed in the H₂OCbl⁺ CD spectrum (Fig. 3B and 3C, center). The γ region again

reveals the presence of at least two electronic transitions, giving rise to the very intense Abs band with a well-developed shoulder on its high-energy side, which is red-shifted by 880 cm⁻¹ with respect to the γ band in the H₂OCbl⁺ spectra (Fig. 3B and 3C).

MeCbl: The dominant features in the ‘unique’ Abs spectrum of MeCbl (Fig. 3A, top) can be similarly classified as those observed in a ‘typical’ Cbl Abs spectrum; however, key differences exist that allow for experimental insight into the effects of

the upper axial ligand on the corrinoid electronic structure. Importantly, the presence of the derivative-shaped features in the α/β region of the CD and MCD spectra (Fig. 3A, center and bottom) suggests that the prominent shoulder on the high-energy side of the β band in the MeCbl Abs spectrum (Fig. 3A, top) corresponds to the origin of another electronic transition. Hence, the α/β region of the Abs spectrum differs from that of ‘typical’ Co³⁺Cbl spectra in that a second relatively intense electronic transition contributes to the Abs spectrum. However, the most unique aspect of the MeCbl Abs spectrum is that the intensity of the γ band is redistributed over three partially resolved features in the UV region that carry similar intensities. Thus the number of electronic transitions in the γ region, similar to the α/β region, also increases from the ‘typical’ to ‘unique’ Co³⁺Cbl spectra.

3.1.2. RR Data

Fig. 4 shows resonance Raman (RR) spectra of H₂OCbl⁺ and MeCbl obtained with 514.5 nm (19436 cm⁻¹) laser excitation. Despite the fact that the two species exhibit markedly different electronic Abs, CD, and MCD spectra (Fig. 3), their RR spectra are strikingly similar. In both cases the dominant features are due primarily to corrin-based vibrations, with the most intense band at \sim 1500 cm⁻¹ corresponding to the long-axis polarized corrin mode ν_{LA} depicted schematically in the inset of Fig. 4. This similarity indicates that substitution of the water ligand in H₂OCbl⁺ by a methyl group in MeCbl does not drastically alter intra-corrin bonding. Intriguingly, however, the 514.5-nm excited RR spectrum of MeCbl exhibits an additional band of significant intensity at 505 cm⁻¹, previously attributed to the Co–C stretching mode ν_{Co-C} [30][31]. Enhancement of this mode upon excitation in resonance with a corrin-based $\pi \rightarrow \pi^*$ transition provides further evidence that the π system of the corrin macrocycle and the Co–C bond are electronically coupled.

3.2. Spectral Analysis

The Abs, CD, and MCD spectra presented in Fig. 3 were iteratively fit with the fewest possible number of Gaussian bands to resolve the major electronic transitions contributing to the Abs spectrum of each Co³⁺Cbl species investigated [1]. The results obtained from Gaussian deconvolutions of the spectra of H₂OCbl⁺, a representative example of a Co³⁺Cbl species exhibiting a ‘typical’ Abs spectrum, and MeCbl, representative of Co³⁺Cbl species displaying a ‘unique’ Abs spectrum, are shown in Fig. 5. While a detailed discussion of the results obtained from this analysis is beyond the scope of this article, the fits are shown here to demonstrate the complemen-

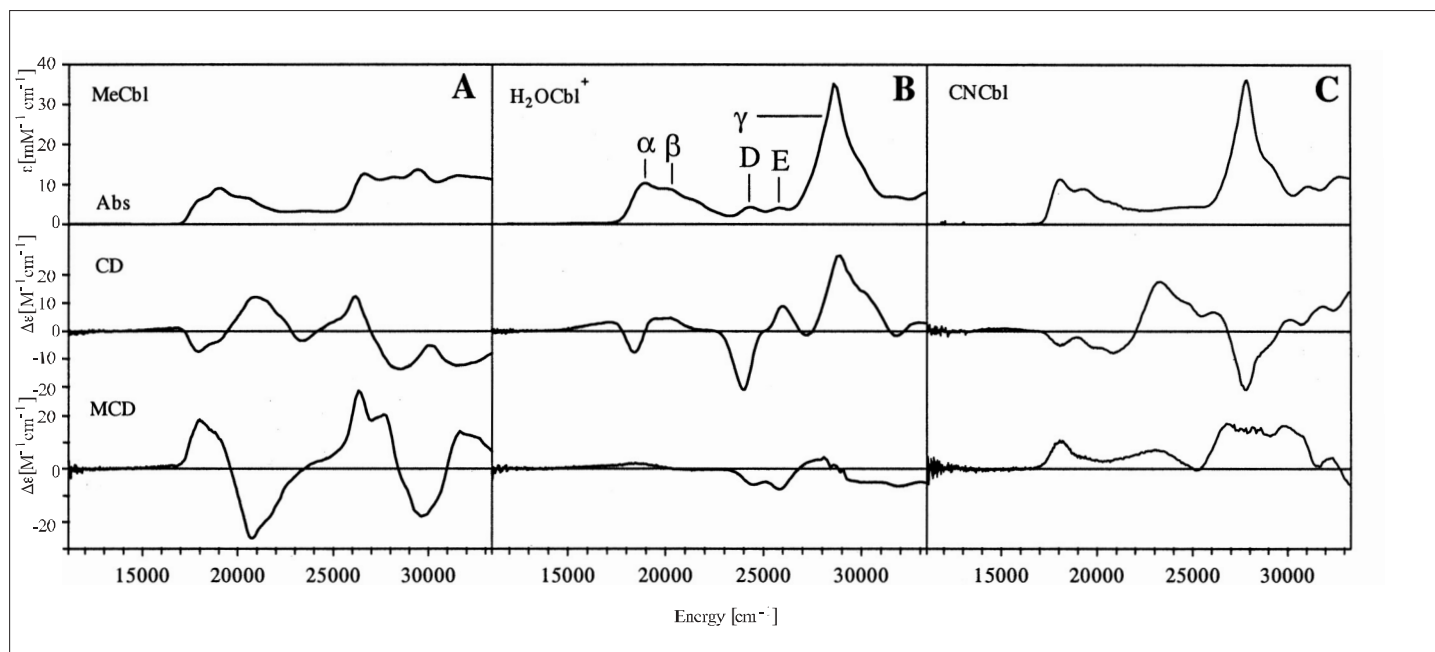


Fig. 3. Absorption (top), CD (center), and 7 T MCD (bottom) spectra recorded at 4.5 K of MeCbl (A), H_2OCbl^+ (B), and CNCbl (C). Band designations are given for H_2OCbl^+ . Reprinted with permission from [1]. Copyright 2003 American Chemical Society.

tary nature of Abs, CD, and MCD data. Clearly, it would be unreasonable to claim that 13 electronic transitions contribute to the spectral region between 15000 and 33000 cm^{-1} based solely on an analysis of the Abs spectrum. However, the fact that the intensities of electronic transitions are governed by different selection rules in Abs, CD, and MCD spectra typically allows electronic transitions that are too weak to be

observed by one technique to be probed using one of the other two methods [26][27]. Knowledge of the exact number of electronic transitions contributing to the Abs spectrum of the species under investigation is crucial, as this information provides an excellent foundation for the rigorous evaluation of computations aimed at generating quantitative bonding descriptions (*vide infra*).

3.3. Computational Data

A number of computational studies of Co^{3+}Cbl have been reported in the recent past, most of which employed the DFT method and relied on the success of geometry optimizations to validate the methodology used [32–34]. However, this approach has the inherent disadvantage that errors are necessarily introduced by using simplified Co^{3+}Cbl models (note that despite significant recent advances in computer technology, treatment of the entire Co^{3+}Cbl cofactor at the DFT level is still unfeasible). Instead, we generated our Co^{3+}Cbl models based on high-resolution X-ray structures [35–37] and used our spectroscopic data in conjunction with the TD-DFT method [38–40] to validate the calculated bonding descriptions [1]. In this evaluation process, a series of TD-DFT calculations were performed on various cofactor models with a variety of functionals and basis sets to find the combination that yielded the best overall agreement between experimental and calculated Abs spectra of H_2OCbl^+ , CNCbl, and MeCbl. While qualitatively similar results were obtained using pure DFT functionals, the B3LYP hybrid functional [41–43] proved most successful in this study as it compensates for the tendency of DFT to overestimate covalent contributions to metal–ligand bonding. To facilitate comparison with our spectroscopic data, TD-DFT computed transition energies and oscillator strengths were used to simulate Abs spectra assuming that each electronic transition gives rise to a Gaussian band of uniform width. Fig. 6 shows that the agreement between calculated and experimental Abs

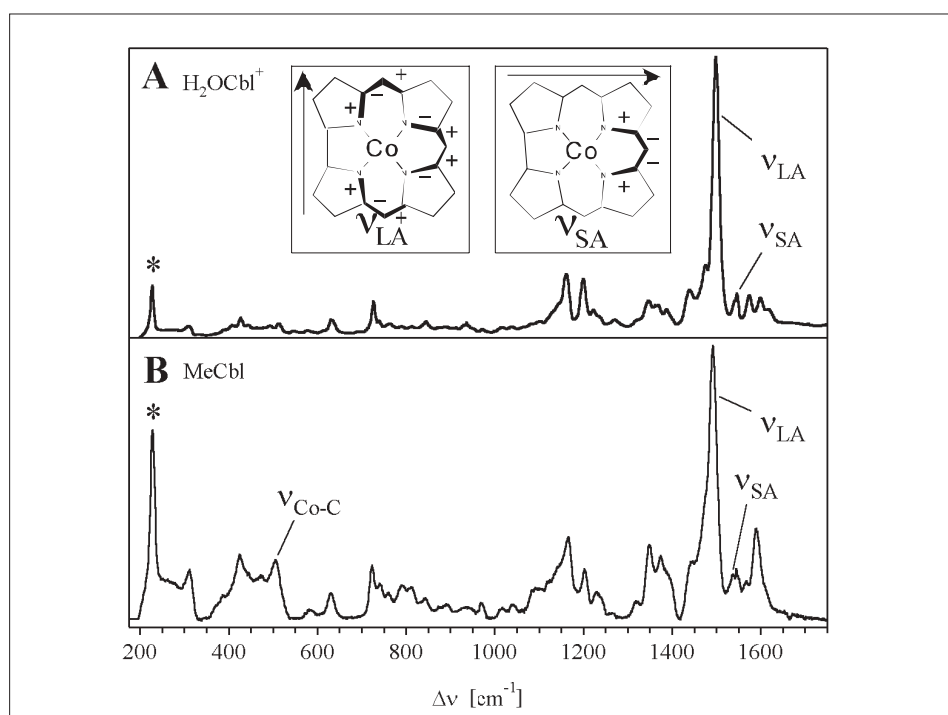


Fig. 4. RR spectra at 77 K of H_2OCbl^+ (A) and MeCbl (B) obtained with 514.5-nm excitation. Insets: Normal mode descriptions and polarizations of ν_{LA} (left) and ν_{SA} (right). Reprinted with permission from [1]. Copyright 2003 American Chemical Society.

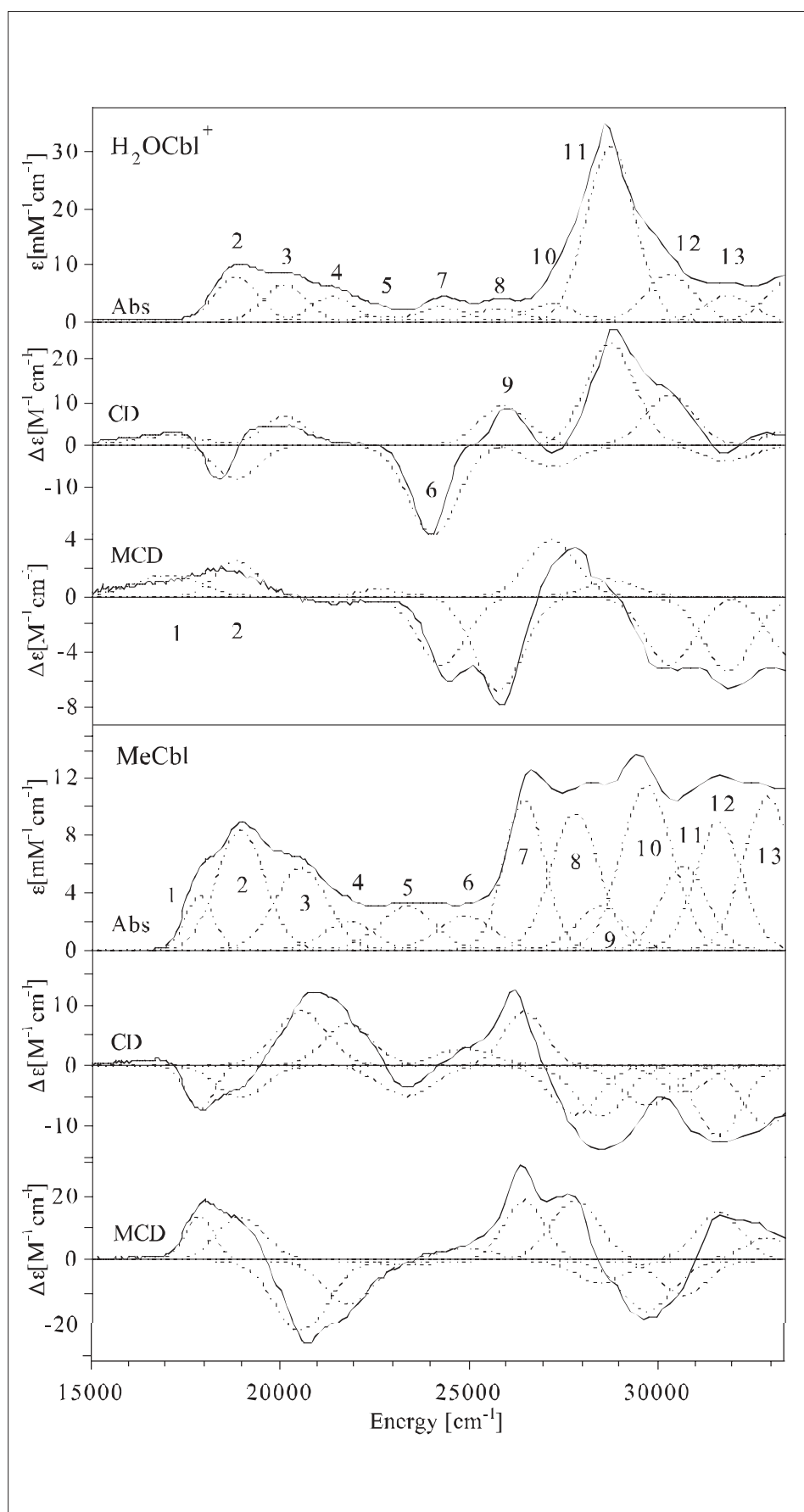


Fig. 5. Solid lines: 4.5 K Abs, CD, and 7 T MCD spectra of H_2OCbl^+ (top 3 panels) and MeCbl (bottom 3 panels). Dotted lines: Gaussian deconvolutions of the experimental spectra. Note that bands 1, 6, and 9 observed in the CD and MCD spectra of H_2OCbl^+ do not appreciably contribute to the Abs spectrum. Reprinted with permission from [1]. Copyright 2003 American Chemical Society.

spectra for all Co^{3+}Cbl species investigated is quite remarkable.

H_2OCbl^+ and CNCbl : For H_2OCbl^+ and CNCbl , our TD-DFT calculations predict one intense electronic transition in the visible spectral region that is polarized along the $\text{C}^5\cdots\text{C}^{15}$ vector of the corrin ring (Fig. 1) and one very intense transition in the UV that is polarized along $\text{Co}\cdots\text{C}^{10}$ vector. Thus the calculations almost quantitatively reproduce the main characteristics of the electronic transitions responsible for the α/β bands and the γ band of 'typical' Abs spectra (Fig. 6A and 6B). Additional transitions carrying lower intensities are predicted near 25000 cm^{-1} where the D and E bands are observed in the experimental Abs spectra. Remarkably, the calculation on the H_2OCbl^+ model also successfully reproduces the weak transition that gives rise to the positive feature on the low-energy side of the α band in the experimental CD spectrum (band 1 in Fig. 5, top).

MeCbl: Our TD-DFT computation on the MeCbl model (Fig. 6C) suggests the presence of two intense features in the α/β region of 'unique' Co^{3+}Cbl Abs spectra, consistent with the results from the Gaussian deconvolutions of our experimental spectra (bands 1/2 and 3/4 in Fig. 5, bottom). Significantly, our TD-DFT calculations also successfully reproduce the dramatic changes in the γ region of the Co^{3+}Cbl Abs spectrum upon substitution of the upper axial ligand by an alkyl group. The calculated 'unique' Abs spectrum of MeCbl shows multiple bands of similar intensities in the UV region where the single intense γ band is predicted (and observed, see Fig. 3) in 'typical' Co^{3+}Cbl spectra.

3.4. Spectral Assignments

As space limitations preclude a detailed discussion of band assignments that emerged from these studies [1], a brief summary of our general strategy that we typically follow to assign key spectral features is given instead. First, the full range of spectroscopic techniques available in our laboratory (Table) is used to experimentally probe the electronic structure of the metal center of interest (as outlined in section 3.1.). Next, a careful spectral analysis is carried out to resolve, and tentatively assign, the major electronic transitions (see section 3.2.). In the following step, computational models are generated and evaluated on the basis of the spectroscopic data and the findings from the corresponding spectral analysis (section 3.3.). Once satisfactory agreement between all calculated and experimental parameters is achieved, indicating that the computed electronic structure description is reasonable, meaningful band assignments can be made based on the computational results. In the present case, the fact that our TD-DFT computed Abs spec-

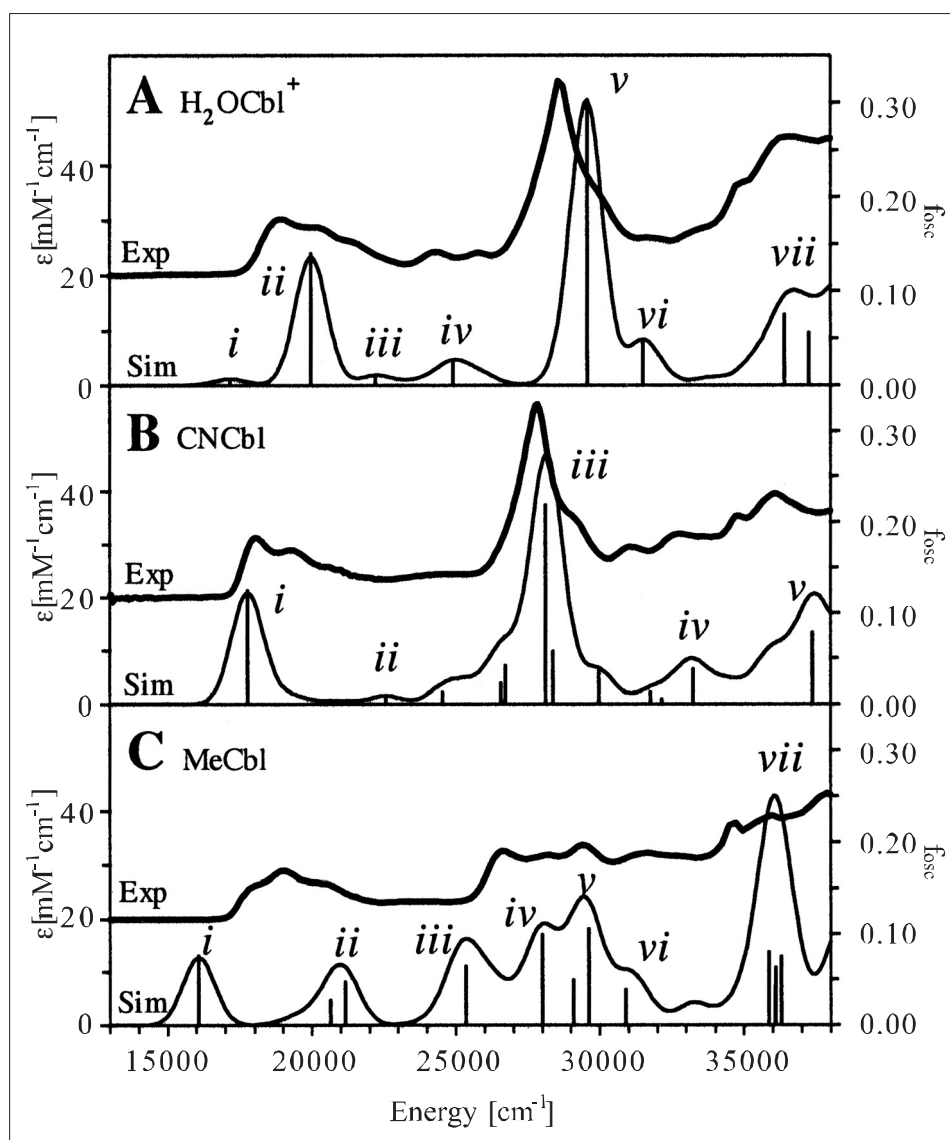


Fig. 6. Experimental and TD-DFT simulated Abs spectra for H_2OCbl^+ (A), CNCbl (B), and MeCbl (C). The calculated spectra were uniformly red-shifted by 5500 cm^{-1} to facilitate comparison with the experimental data. The transitions producing the dominant contributions to the calculated spectra are indicated by solid lines (the corresponding oscillator strengths are given on the right-hand axis). Reprinted with permission from [1]. Copyright 2003 American Chemical Society.

tra for H_2OCbl^+ , CNCbl , and MeCbl reproduce all essential features observed in the corresponding experimental data and properly predict the obvious experimental trends (such as the correlated shifts of the α/β and γ bands and the intensity redistribution in the γ region as a function of the upper axial ligand) permitted us to use the DFT calculated MO descriptions as the basis for assigning the relevant spectral features in both the 'typical' and the 'unique' Abs spectra of Co^{3+}Cbl s. These assignments are briefly summarized below.

4. Discussion

Spectroscopic data of corrinoids reported in the literature are abundant. However, despite numerous decades of intensive in-

vestigations of the B_{12} cofactors MeCbl and AdoCbl , their 'unique' Abs spectra remained largely unassigned [25]. Likewise, geometric and electronic factors distinguishing Co^{3+}Cbl species exhibiting 'typical' Abs spectra from those displaying 'unique' Abs spectra had yet to be explored. To address these issues, we have developed a combined spectroscopic/computational methodology to probe the ground and excited electronic states of representative Co^{3+}Cbl species exhibiting 'typical' and 'unique' Abs spectra [1]. Below, key findings from these studies are briefly discussed and their implications for biological Co–C bond activation are explored.

Co³⁺Cbl Species Exhibiting 'Typical' Abs Spectra: Our TD-DFT-assisted analysis of the 'typical' H_2OCbl^+ and CNCbl Abs spectra (Fig. 3) reveals that the α and β

bands correspond to the electronic origin and the first member of a progression in ν_{LA} (depicted in the inset of Fig. 4) associated with the corrin-based HOMO \rightarrow LUMO transition that is polarized along the $\text{C}^5\cdots\text{C}^{15}$ vector (Fig. 1). The most intense transition in the D/E region is assigned to a corrin-based $\pi \rightarrow \pi^*$ transition from the HOMO–1 to the LUMO. Lastly, the single intense transition responsible for the prominent γ band in these spectra is also attributed to a corrin-based $\pi \rightarrow \pi^*$ transition originating from the HOMO. The primary acceptor orbital in this transition is a corrin π^* orbital that has the same symmetry as the HOMO with respect to the approximate C_s mirror plane of the corrin macrocycle (Fig. 1), which results in a transition moment that is oriented roughly along the $\text{Co}\cdots\text{C}^{10}$ vector.

As cyanide is a much stronger σ -donor than a water molecule, our DFT calculations predict that the Co $3d_{z^2}$ -based MO is considerably raised in energy in CNCbl relative to H_2OCbl^+ , consistent with the $\sim 1.42\text{ V}$ lower reduction midpoint potential of the former [44][45]. Additionally, the contribution from the formally unoccupied Co $3d_{z^2}$ orbital to the corrin-based HOMO increases from 0.2% in H_2OCbl^+ to 1.5% in CNCbl . This partial population of the Co $3d_{z^2}$ orbital induces a strong σ -antibonding interaction between the cobalt and the coordinated nitrogen of the lower axial base (N_{ax}), thereby raising the energy of the HOMO and lowering the energies of electronic transitions originating from this orbital. Thus our DFT calculations afford an intuitively appealing model for explaining the long-established trend that the α/β and γ bands in 'typical' Co^{3+}Cbl Abs spectra uniformly shift to lower energy with increasing σ -donor strength of the upper axial ligand [25].

Co³⁺Cbl Species Exhibiting 'Unique' Abs Spectra: Binding of an alkyl ligand in the upper axial position of Co^{3+}Cbl s, as in MeCbl and AdoCbl , results in the appearance of a significantly perturbed, 'unique' Co^{3+}Cbl Abs spectrum (Fig. 3). Our DFT computations on MeCbl indicate that these spectral changes reflect the increased σ -donor strength of the alkyl ligand and the consequent destabilization of all Co $3d$ orbitals. As a result, the occupied Co $3d$ orbitals of MeCbl and, presumably, alkylcobalamins in general, shift close in energy to the HOMO, which gives rise to (i) a net increase in the number of donor MOs available for electronic transitions and (ii) extensive mixing between Co $3d$ and corrin π orbitals. It is the combination of these two effects that is responsible for the 'unique' Abs spectra of alkylcobalamins.

The greater σ -donor strength of the upper axial ligand in MeCbl compared to CNCbl and H_2OCbl^+ leads to a further in-

crease in Co $3d_{z^2}$ orbital character in the corrin-based HOMO to 6.7%, thereby inducing an even stronger Co–N_{ax} σ -antibonding interaction. As a result, the DFT calculated Co–N_{ax} bond order decreases from 0.65 in H₂OCbl⁺ to 0.42 in CNCbl and 0.35 in MeCbl. These values correlate nicely with the experimental Co–N_{ax} bond lengths that increase from 1.925 Å in H₂OCbl⁺ [37] to 2.041 Å in CNCbl [35] and 2.162 Å in MeCbl [35]. Consequently, the model used to explain shifts in the α band position can also be invoked to rationalize the observed lengthening of the Co–N_{ax} bond with increasingly stronger σ -donors in the upper axial position [46].

Nature of the Co–C Bond and Implications for Co–C Bond Activation: The mechanism by which MeCbl- and AdoCbl-dependent enzymes activate the cofactor's Co–C bond to produce a methyl cation and an Ado[•] radical, respectively, is an enduring subject of intense research [20][28] [47–50]. Our DFT-generated electronic-structure description for MeCbl indicates that the Co–CH₃ bond is very covalent, as revealed by the large methyl C $2p_z$ orbital character of 22% in the unoccupied Co $3d_{z^2}$ -based MO. Since the methyl C $2p_z$ -derived occupied counterpart (*i.e.* the Co–C σ -bonding MO) is in close energetic proximity to the corrin-based HOMO, these two MOs are strongly mixed. Consequently, the

HOMO of MeCbl exhibits substantial Co–C σ -bonding character, thus potentially offering the opportunity to modulate the properties of the organometallic bond through corrin ring deformations. However, because this electronic coupling only involves weak π -interactions, conformational changes of the corrin macrocycle are not expected to perturb the Co–CH₃ bond to any significant degree.

A puzzling and previously poorly understood result from earlier studies of Co³⁺corrinoids is that while the identity of the upper axial ligand has a great effect on the Co–N_{ax} bond strength, the lower axial ligand does not appreciably modulate the Co–C bond strength. Significantly, our DFT computations also provide a simple explanation for this phenomenon, summarized pictorially by the qualitative MO diagram in Fig. 7. While substitution of the upper axial ligand from H₂OCbl⁺ to MeCbl induces a substantial Co–N_{ax} σ -antibonding interaction and, consequently, a weakening of this bond, replacement of the lower axial DMB ligand of MeCbl by a water molecule in methylcobinamide (MeCbi⁺) has virtually no effect on the Co–C bond (*i.e.* the bond order does not change, as both occupied MOs are σ -bonding with respect to the Co–C bond). In support of this model, RR experiments by Spiro and coworkers revealed that the Co–C bond strengths in

MeCbl and MeCbi⁺ are virtually identical [30][31].

These results have important implications with respect to possible Co–C bond activation mechanisms employed by B₁₂-dependent enzymes, as they argue strongly against models invoking involvement of the lower axial ligand. For such a mechanism to be operative, it would be necessary for the σ -donor strength of the lower axial ligand to exceed that of the alkyl ligand, in which case the central MO of MeCbl in Fig. 7 would become σ -antibonding with respect to the Co–C bond (rather than the Co–N_{ax} bond). However, this possibility can be ruled out since X-ray structural data of B₁₂-dependent enzymes reveal that the lower axial position is occupied by either the DMB or a histidine residue, both of which are considerably weaker σ -donors than alkyl ligands. Consequently, as more results become available, it seems less and less likely that enzymatic Co–C bond activation involves corrin ring deformation and/or electronic perturbations induced by the lower axial ligand. Rather, a mechanism invoking stabilization of the Co–C bond cleavage products; *i.e.* the Co¹⁺Cbl species and the Co²⁺Cbl/Ado[•] radical pair in the case of MeCbl and AdoCbl dependent enzymes, respectively, seems more plausible [51].

Acknowledgment

The author thanks Troy A. Stich and Amanda J. Brooks whose hard work this article reflects, and acknowledges the University of Wisconsin and the NSF (CAREER grant MCB-0238530) for financial support of this project.

Received: February 13, 2004

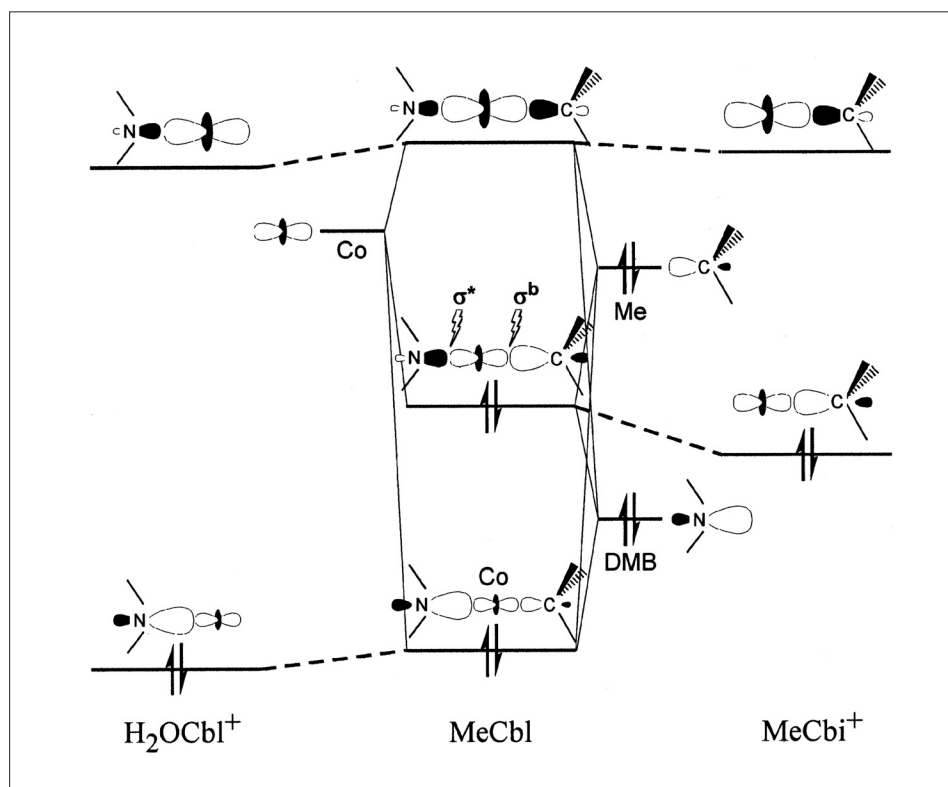


Fig. 7. Qualitative correlation diagram describing the bonding interactions between the cobalt center and the axial ligands in H₂OCbl⁺ (left), MeCbl (center), and MeCbi⁺ (right). Reprinted with permission from [1]. Copyright 2003 American Chemical Society.

- [1] T.A. Stich, A.J. Brooks, N.R. Buan, T.C. Brunold, *J. Am. Chem. Soc.* **2003**, *125*, 5897–5914.
- [2] R. Banerjee (Ed.), 'Chemistry and Biochemistry of B₁₂', Wiley-Interscience, New York, **1999**.
- [3] R. Banerjee, *Biochemistry* **2001**, *40*, 6191–6198.
- [4] D. Dolphin (Ed.), 'B₁₂', Wiley, New York, **1982**.
- [5] M.L. Ludwig, C.L. Drennan, R.G. Matthews, *Structure* **1996**, *4*, 505–512.
- [6] M.L. Ludwig, R.G. Matthews, *Annu. Rev. Biochem.* **1997**, *66*, 269–313.
- [7] D.C.P.J. Hodgkin, J.H. Robertson, K.N. Trueblood, R.J. Prosen, J.G. White, *Nature* (London) **1956**, *176*, 325.
- [8] R.G. Finke, B.P. Hay, *Inorg. Chem.* **1984**, *23*, 3041.
- [9] R. Banerjee, *Chem. Biol.* **1997**, *4*, 175–186.
- [10] R.G. Matthews, *Acc. Chem. Res.* **2001**, *34*, 681–689.
- [11] C.L. Drennan, S. Huang, J.T. Drummond, R.G. Matthews, M.L. Ludwig, *Science* **1994**, *266*, 1669–1674.
- [12] C.L. Drennan, R.G. Matthews, M.L. Ludwig, *Curr. Opin. Struct. Biol.* **1994**, *4*, 919–929.

- [13] N.H. Thoma, P.R. Evans, P.F. Leadlay, *Biochemistry* **2000**, *39*, 9213–9221.
- [14] N.H. Thoma, P.F. Leadlay, *Protein Sci.* **1996**, *5*, 1922–1927.
- [15] F. Mancina, P.R. Evans, *Struct. Fold. Des.* **1998**, *6*, 711–720.
- [16] G.J. Gerfen, S. Licht, J.-P. Willems, B.M. Hoffman, J. Stubbe, *J. Am. Chem. Soc.* **1996**, *118*, 8192–8197.
- [17] O.T. Magnusson, G.H. Reed, P.A. Frey, *Biochemistry* **2001**, *40*, 7773–7782.
- [18] K.L. Brown, X. Zou, *J. Inorg. Biochem.* **1999**, *77*, 185–195.
- [19] B.P. Hay, R.G. Finke, *J. Am. Chem. Soc.* **1986**, *108*, 4820–4829.
- [20] S. Chowdhury, R. Banerjee, *Biochemistry* **2000**, *39*, 7998–8006.
- [21] B.P. Hay, R.G. Finke, *J. Am. Chem. Soc.* **1987**, *109*, 8012–8018.
- [22] Z. Schneider, A. Stroinski, 'Comprehensive B12: Chemistry, Biochemistry, Nutrition, Ecology and Medicine', De Gruyter, New York, **1987**.
- [23] R.A. Firth, H.A.O. Hill, J.M. Pratt, R.J.P. Williams, W.R. Jackson, *Biochemistry* **1967**, *6*, 2178–2189.
- [24] A.M. Calafat, S. Taoka, J.M. Puckett, C. Semerad, H. Yan, L.B. Luo, H.L. Chen, R. Banerjee, L.G. Marzilli, *Biochemistry* **1995**, *34*, 14125–14130.
- [25] J.M. Pratt, in 'Chemistry and Biochemistry of B12', Ed. R. Banerjee, Wiley, New York, **1999**, pp 113–164.
- [26] E.I. Solomon, M.L. Kirk, D.R. Gamelin, S. Pulver, *Methods in Enzymology* **1995**, *246*, 71–110.
- [27] E.I. Solomon, M.A. Hanson, in 'Inorganic Electronic Structure and Spectroscopy', Eds. E.I. Solomon, A.B.P. Lever, Wiley, New York, **1999**, Vol. 2, pp 1–130.
- [28] F. Neese, E.I. Solomon, *Inorg. Chem.* **1999**, *38*, 1847–1865.
- [29] S. Salama, T.G. Spiro, *J. Raman Spec.* **1977**, *6*, 57–60.
- [30] S.L. Dong, R. Padmakumar, R. Banerjee, T.G. Spiro, *J. Am. Chem. Soc.* **1996**, *118*, 9182–9183.
- [31] S.L. Dong, R. Padmakumar, R. Banerjee, T.G. Spiro, *Inorg. Chim. Acta* **1998**, *270*, 392–398.
- [32] K.P. Jensen, S.P.A. Sauer, T. Liljefors, P.O. Norrby, *Organometallics* **2001**, *20*, 550–556.
- [33] M.P. Jensen, J. Halpern, *J. Am. Chem. Soc.* **1999**, *121*, 2181–2192.
- [34] M.P. Jensen, D.M. Zinkl, J. Halpern, *Inorg. Chem.* **1999**, *38*, 2386–2393.
- [35] L. Randaccio, M. Furlan, S. Geremia, M. Slouf, I. Srnova, D. Toffoli, *Inorg. Chem.* **2000**, *39*, 3403–3413.
- [36] J.P. Bouquiere, J.L. Finney, M.S. Lehmann, P.F. Lindley, H.F.J. Savage, *Acta Crystallogr. Sect. B-Struct. Commun.* **1993**, *49*, 79–89.
- [37] C. Kratky, G. Farber, K. Gruber, K. Wilson, Z. Dauter, H.F. Nolting, R. Konrat, B. Kräutler, *J. Am. Chem. Soc.* **1995**, *117*, 4654–4670.
- [38] R. Bauernschmitt, R. Ahlrichs, *Chem. Phys. Lett.* **1996**, *256*, 454.
- [39] E.M. Casida, C. Jamorski, K.C. Casida, D.R. Salahub, *J. Chem. Phys.* **1998**, *108*, 4439.
- [40] R.E. Stratman, G.E. Scuseria, M.J. Frisch, *J. Chem. Phys.* **1998**, *109*, 8218.
- [41] A.D. Becke, *J. Chem. Phys.* **1993**, *98*, 1372.
- [42] A.D. Becke, *J. Chem. Phys.* **1993**, *98*, 5648.
- [43] C. Lee, W. Yang, R.G. Parr, *Phys. Rev. B* **1988**, *37*, 785.
- [44] B. Jaselskis, H. Diehl, *J. Am. Chem. Soc.* **1954**, *76*, 4345–4348.
- [45] O. Muller, G. Muller, *Biochem. Zeit.* **1962**, *336*, 299.
- [46] J.M. Pratt, in 'Chemistry and Biochemistry of B12', Ed. R. Banerjee, Wiley, New York, **1999**, pp 73–112.
- [47] S. Chowdhury, R. Banerjee, *J. Am. Chem. Soc.* **2000**, *122*, 5417–5418.
- [48] K.L. Brown, J. Zou, *J. Am. Chem. Soc.* **1998**, *120*, 9466–9474.
- [49] S.L. Dong, R. Padmakumar, R. Banerjee, T.G. Spiro, *J. Am. Chem. Soc.* **1999**, *121*, 7063–7070.
- [50] B. Kräutler, W. Keller, C. Kratky, *J. Am. Chem. Soc.* **1989**, *111*, 8936–8938.
- [51] A.J. Brooks, M. Vlasie, R. Banerjee, T.C. Brunold, *J. Am. Chem. Soc.* **2004**, submitted.